ACS Photonics

Article

pubs.acs.org/journal/apchd5

Graphene Oxide/Gold Nanorod Nanocomposite for Stable Surface-Enhanced Raman Spectroscopy

Pilar G. Vianna,[†] Daniel Grasseschi,[†] Greice K. B. Costa,[‡,§] Isabel C. S. Carvalho,[‡] Sergio H. Domingues,[†] Jake Fontana,[⊥] and Christiano J. S. de Matos*[,†]

[†]MackGraphe – Graphene and Nanomaterials Research Center, Mackenzie Presbyterian University, São Paulo – 01302-907, Brazil

[‡]Department of Physics, Pontifícia Universidade Católica do Rio de Janeiro, Rio de Janeiro – 22451-900, Brazil

[§]Photonic and Instrumentation Laboratory, UFRJ, Rio de Janeiro – 21941-598, Brazil

[⊥]Naval Research Laboratory, 4555 Overlook Avenue SW, Washington D.C. 20375, United States

Supporting Information

ABSTRACT: We introduce a graphene oxide/gold nanorod nanocomposite as a surface-enhanced Raman spectroscopy (SERS) substrate that suppresses the usual temporal intensity fluctuations, commonly referred to as blinking. The temporal stability of the SERS spectra from the nanocomposite is statistically determined using the coefficient of variation of the integrated spectra. We demonstrate that, by introducing graphene oxide, the coefficient of variation from the nanocomposite is five times smaller when compared to gold nanorods without graphene oxide, which is attributed to the removal of the nanorod's surfactant from plasmonic hot spots due to graphene oxide–surfactant interaction. The resulting nanocomposite can, then, be used as a reliable substrate for precise SERS chemical analysis. The nanocomposite is, therefore, analyzed as a SERS substrate for the detection of Rhodamine 640, providing a 4-fold stability improvement relative to gold nanorods without graphene oxide, while the dye's Raman signal is enhanced both by SERS and by resonant excitation.

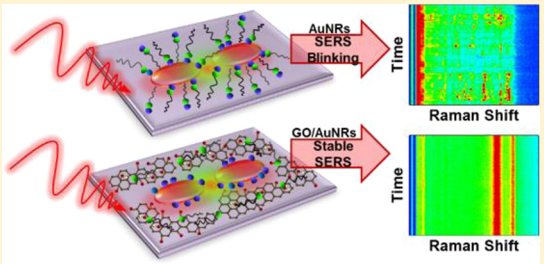

KEYWORDS: *graphene oxide, gold nanorods, nanocomposite, SERS, blinking*

Surface-enhanced Raman spectroscopy (SERS) is a robust and precise approach for molecular detection. The sensitivity of the technique can enable single molecule identification, thus supporting the investigation of molecular dynamics and fundamental properties not inferable on an ensemble of molecules.[1−8] The large detection sensitivity primarily arises via an electromagnetic mechanism (EM).[9−12] When light is incident onto plasmonic nanostructures, free electrons on the surface of the nanoparticles are concentrated to the sharp edges, leading to electromagnetic "hot spots" and enhancement of the local electric field, E. If a molecule is placed in the vicinity of these hot spots, the Raman scattering intensity from the molecule can be significantly amplified, scaling as E^4.[13,14] Thus, anisotropic plasmonic nanoparticles such as gold nanorods (AuNRs) make excellent candidates for SERS. The AuNR synthesis commonly employs cetyltrimethylammonium bromide (CTAB), a cationic surfactant that acts as a directing and stabilizing agent controlling the crystal growth process and prevents nanorods aggregation. While the surfactant is of ultimate importance in determining the rod's size and shape,[10−12] it can, as any surfactant, severely interfere with the detection of other molecules[9,11] due to the intensity of the SERS signal falling off as r^{-10} from the surface of the nanoparticle.[14] Additionally, this prevents stronger interaction with analyte molecules and inhibits charge transfer, which would further increase SERS sensitivity via the process known as the chemical mechanism (CM).

Unlike the case of CTAB-stabilized nanorods, charge transfer is believed to be significant when graphene-based materials are used as substrates, and CM-SERS has been reported for the detection of various molecules such as crystal violet, phthalocyanine, Rhodamine 6G, Rhodamine B, and proto-porphyrin IX.[15,16] Furthermore, graphene-based materials/metallic nanostructure hybrids are of special importance to SERS, as they may provide higher enhancement factors,[17] as well as improved system reproducibility[18] and adsorption to certain target molecules. Hu et al., for example, reported a graphene oxide (GO)/AuNR nanocomposite for the detection of aromatic dye molecules, demonstrating the Raman enhancement of specific probes due to the electrostatic interaction between GO and different charged molecules.[18] In addition, GO has been reported to assist with the removal of ligands and surfactants, including CTAB,[19] from the surface of gold[19] and silver[20,21] nanocrystals attached to it, which has been exploited to induce the reshaping of the nanocrystals. GO has also been reported to allow for the in situ growth of metal nanoparticles,[22,23] thus, preventing aggregation without the need of

Received: February 15, 2016
Published: May 9, 2016

DOI: 10.1021/acsphotonics.6b00109
ACS Photonics 2016, 3, 1027−1035

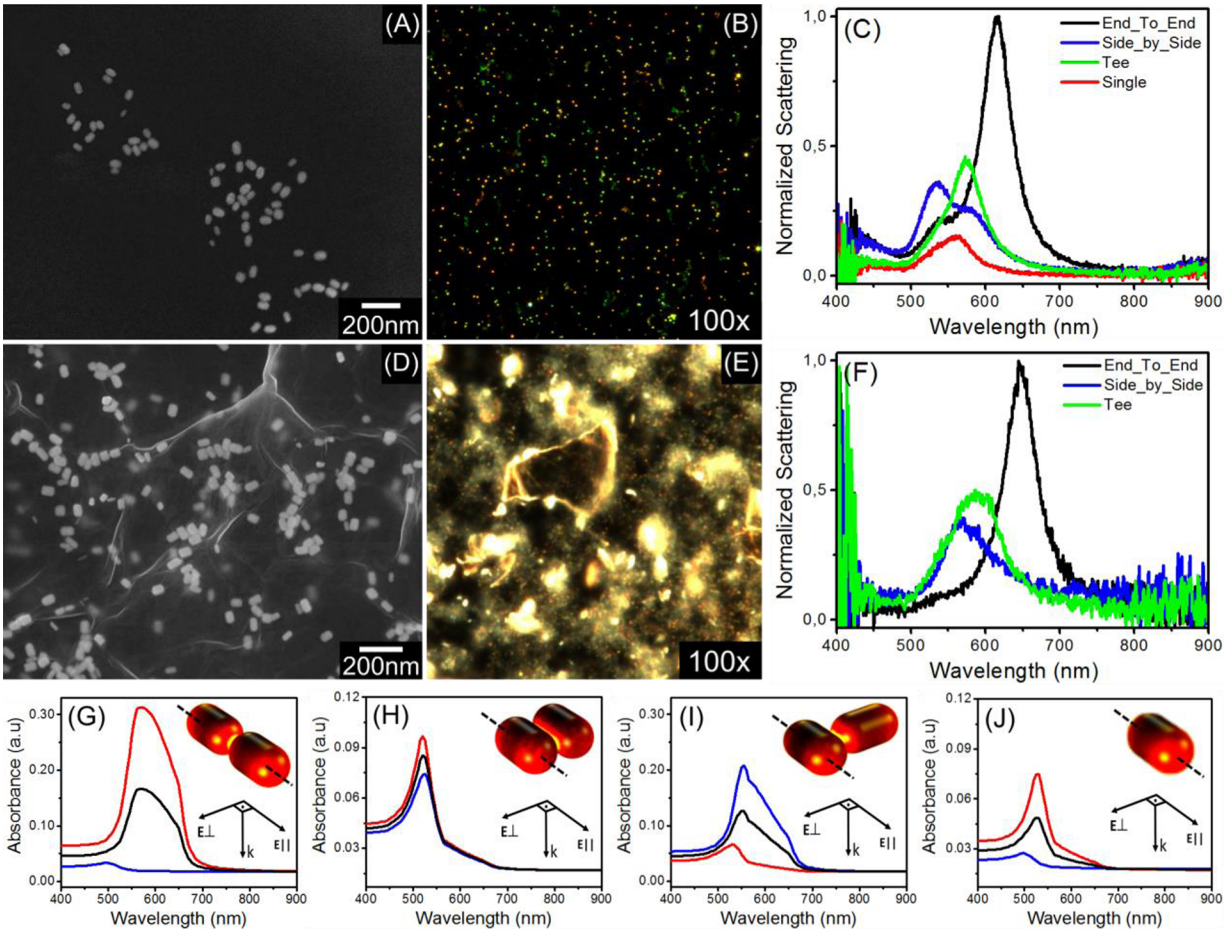

Figure 1. Morphological and optical characterization of the AuNR (a–c) and GO/AuNR samples (d–f). (a, d) SEM images; (b, e) dark-field optical microscopy images; (c, f) Rayleigh scattering spectra at points with different nanorod dimer orientations and for a single nanorod (for the AuNR case only); (g–j) Simulated absorbance spectra of the AuNR sample for different dimer orientations and single nanorod (insets). The average absorbance and the absorbance for the perpendicular and parallel electric field configurations are shown as the black, blue, and red curves, respectively.

surfactants. However, this method does not allow for the precise control of the morphology of the particles.[17]

Despite its benefits, the sensitivity enhancement offered by SERS also leads to strong temporal fluctuations in the intensity and spectral position of Raman lines.[6,24,25] This issue, which became known as blinking, can lead to poor molecular recognition and has largely prevented the widespread practical application of SERS in areas that require high accuracy standards, such as chemical sensing[7] and medical diagnosis.[12,26] While the blinking dynamics has not yet been fully understood, a variety of physical and chemical processes have been suggested.[3,7,8,24,25,27,28] Molecular diffusion and adsorption/desorption cycles within a hot spot are among the most accepted pictures.[24,25,27] However, it has also been mentioned that temporal changes in the configuration of the SERS substrate, leading to changes in the position and strength of hot spots, may also cause intense instabilities.[8] In such cases, the surfactant on metallic nanocrystals can play a significant role. Indeed, Mezni et al. showed that two distinct stabilizing agents (PVP and TREG), used in the preparation of triangular gold nanoprisms, induce intense signal fluctuation due to the molecular dynamic exchange of these species on the prisms' surface.[28] We note that citrate-stabilized gold nanoparticles usually offer more stable SERS spectra, but at the expense of (and partially due to) a lower EM gain achieved with the spherical shape obtained in this case. Indeed, blinking and citrate signal interference have been reported for citrate-synthesized silver nanoparticles, which present higher SERS gains.[25,29] We also note that, so far, the blinking issue has not been addressed in nanocomposites composed of graphene-based materials and metallic nanoparticles.

In this work, we demonstrate blinking suppression in a nanocomposite consisting of GO and AuNRs. While the SERS spectra obtained with AuNRs without GO or analyte molecules exhibited strong blinking attributed to CTAB, the GO/AuNR nanocomposite was found to suppress the CTAB signal and its temporal instability. The nanocomposite was then successfully used as a SERS substrate for the detection of Rhodamine 640 (RH640) at concentrations as low as 10^{-10} M. The resulting signal presented excellent stability, with well-defined and blinking-free RH640 Raman modes detected.

RESULTS AND DISCUSSION

Sample Characterization. AuNRs were synthesized by a seed-mediated method using CTAB as the capping agent,[30] while GO was prepared by a modified Hummers method[31] (for details, see Methods). The GO/AuNR nanocomposite was then prepared by dipping a substrate into the GO suspension, drying it with N_2, and subsequently dipping it into the AuNRs suspension (see Methods). Alternatively drop casting a

DOI: 10.1021/acsphotonics.6b00109
ACS Photonics 2016, 3, 1027–1035

previously stirred GO/AuNRs suspension yielded similar results (not shown). For characterization, scanning electron microscopy (SEM) and confocal Raman spectroscopy were carried out on samples that were prepared on silicon wafers with a 300 nm thick silicon oxide top layer, while glass slides were used for dark-field optical microscopy and spectroscopy measurements. The characterization results with AuNR-only and with GO/AuNR samples are depicted in Figure 1.

Figure 1a shows a SEM image of a sample comprising AuNRs only. Nanorods with an average length and diameter of 60.1 ± 0.5 nm and 35.0 ± 0.4 nm, respectively, can be observed. Figure 1d shows a GO/AuNR sample with roughly the same average dimensions (length/diameter of 59.4 ± 0.5 nm/33.0 ± 0.3 nm), indicating that the composite formation does not significantly affect the AuNRs shape. The image also shows that the nanocomposite presents an aspect that is similar to those previously reported in the literature[18,19,32−34] and indicates that the AuNRs are well attached to both sides of the GO sheets, which is believed to be a consequence of the electrostatic attraction between the negatively charged GO sheets and the positive charge of the cationic (CTA^+) on the gold surface.[18,19,33,35]

Figure 1b shows a dark-field image of the AuNR sample. Different points across the sample present different colors, which are associated with the four distinct Rayleigh scattering spectra shown in Figure 1c. The shapes and relative positions of these spectra bear great resemblance to those reported by Funston et al.[36] and can be assigned to isolated AuNRs and to three different AuNRs dimer configurations: tee, end-to-end, and side-by-side. Funston et al. show that end-to-end dimmers present the most intense scattering peaks, with the largest red shifts relative to isolated rods; tee dimers show a smaller red shift, while side-by-side dimers present a blue shift. These trends were also confirmed by electromagnetic simulations (Figures 1g−j). For computational simplicity, the S_{21} element from the scattering matrix was retrieved from simulations and used to calculate the absorbance spectra. According to Gans theory, which is an extension of Mie theory for cylindrical or oblate particles, the absorption and scattering cross sections are expected to present the same profile, with the latter red-shifted by a few nanometers.[37,38]

The end-to-end aggregation (inset of Figure 1g) is found to yield the highest number of counts in the dark-field images, corresponding to 77% of the detected scattering sites. It corresponds to the yellow, orange and red spots in the dark-field image (see Supporting Information), with the precise color depending on the exact rod-to-rod distance. Simulations also show that this configuration yields the highest scattering strength (Figure 1g), associated with the highest enhancement factor in SERS. Figure 1e,f shows a dark-field image and Rayleigh scattering spectra obtained with the GO/AuNR sample. Although Figure 1e shows significant levels of scattering from borders and folds of GO flakes, the colored points, associated with the AuNRs, are still visible. In fact, due to the intense GO scattering, the illumination intensity had to be reduced by 50% to avoid saturation in the camera. This reduction, together with the competing GO scattering spectra, accounts for the higher signal-to-noise ratio observed in the nanocomposite's normalized dark-field spectra (see Supporting Information). As a consequence, the single-rod scattering spectrum could not be distinguished from noise in the composite. Nevertheless, direct comparison between the scattering intensities for the AuNR and GO/AuNR samples indicates that similar plasmonic field enhancements are achieved in both cases.

In the GO/AuNR nanocomposite scattering spectra (Figure 1f), the three dimer spectral profiles are still present, indicating that GO does not change the nanorods' aggregation condition, which is also evidenced by the SEM image (Figure 1d). Compared with Figure 1c, a redshift of the plasmon resonance bands is observed, which can be associated with changes in the dielectric constant around the AuNRs in the nanocomposite.[9,39] This provides further evidence of the composite formation, with the distance between GO and the AuNRs necessarily being of a few nanometers at most.[18] Further evidence of the GO-AuNR attachment was given by the fact that in the dark-field images of the AuNRs it was possible to notice particles in Brownian motion, that is, not attached to the substrate. In contrast, in the GO/AuNR sample, moving particles were not observed, even within a wet sample, indicating they were adsorbed to the GO surface.

The SERS signal from the samples, as well as its temporal stability, was then measured. A laser line of 633 nm was used to take advantage of the observed plasmon resonances. The AuNR sample was found to exhibit strong temporal oscillation (blinking). The assignment of the SERS bands under these circumstances is usually not an easy task,[28] as sudden vanishing, broadening, or intensification of the bands make molecular fingerprint identification rather difficult. Figure 2 illustrates a single spectrum of the AuNR sample acquired with an integration time of 200 s and a laser power of 70 μW. Comparison with the Raman spectrum of pure CTAB powder was made, and the marked peaks (asterisks) in Figure 2 refer to the tentative assignment to known CTAB Raman modes. The peak at 179 cm^{-1} (red asterisk) is attributed to the Au−Br stretching mode,[40,41] indicating a chemical bond between CTAB and the AuNRs. The large number of assigned peaks confirms that the SERS spectrum is that of CTAB (see Supporting Information). The shown spectrum was normalized by the highest significant peak, and the background was not removed, as it has been shown to be strongly correlated to the blinking effect.[2,25,42]

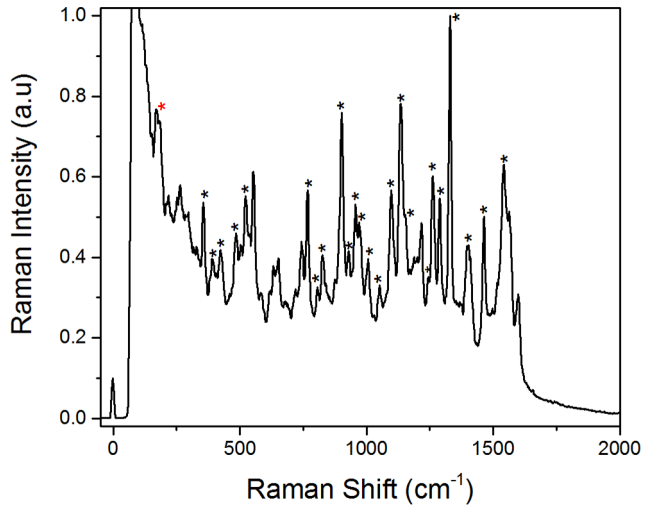

Figure 2. SERS spectrum of the AuNR sample acquired with an integration time of 200 s and the 633 nm excitation wavelength. The asterisks indicate the modes that are successfully assigned to CTAB. The red asterisk denotes the Au−Br stretching mode.

DOI: 10.1021/acsphotonics.6b00109
ACS Photonics 2016, 3, 1027−1035

Figure 3a and b show normalized Raman spectrum time series for the AuNR and GO/AuNR nanocomposite samples

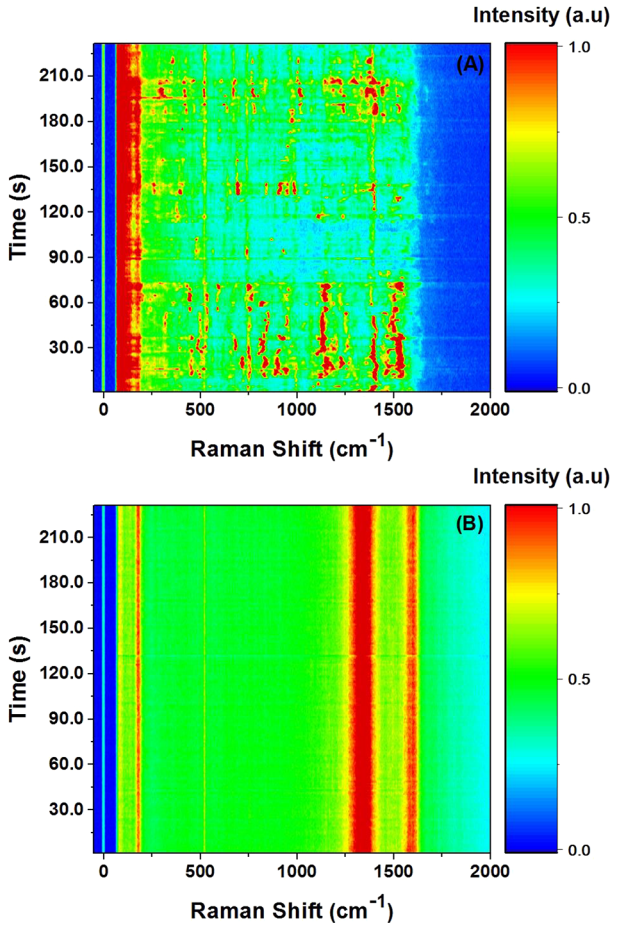

Figure 3. SERS spectra time series for the (a) AuNR sample and (b) GO/AuNR nanocomposite sample.

under laser powers of 0.21 and 0.34 mW, respectively. It is evident from Figure 3a that the AuNR sample exhibits strong SERS blinking. In contrast, temporally stable spectra are shown in Figure 3b, with the characteristic D and G bands of GO appearing at 1335 and 1595 cm^{-1}, respectively. While the 179 cm^{-1} Au−Br band is visible, all other CTAB peaks do not appear. GO is recognized for its ability to adsorb long-chain molecules.[20] In fact, CTAB is known to self-assemble on GO's surface either through van der Waals forces between its hydrocarbon tails or via electrostatic attraction between the negatively charged GO and the cationic CTAB polar head groups.[35,43] We then speculate that CTA$^+$ is electrostatically attracted by and displaced toward GO, while the bromide remains in the AuNRs' surface due to its high affinity to gold atoms and its soft base characteristic.[44] The bromide presence may help maintain the AuNRs shape,[9] as indeed observed, meaning that the rod's plasmonic properties are preserved. The absence of CTA$^+$ Raman bands indicates its removal from the plasmonic hot spots on the AuNRs' surface, as a consequence of its interaction with GO.

It is noted that the blinking phenomenon observed in Figure 3a, as well as all CTAB Raman peaks (including the Au−Br peak in Figure 3b) are only visible under 633 nm laser line excitation. Out of plasmon resonance (at 488 nm), only the Si (substrate) line and the GO bands are obtained in the AuNR and GO/AuNR samples, respectively (see Supporting Information). The resonant enhancement of the Au−Br Raman band is, therefore, strong evidence of the presence of the AuNRs on the GO surface. Using a 532 nm laser line, although the AuNRs are still in the plasmonic resonance, the imaginary part of gold's dielectric constant is large, causing reabsorption of the scattered photons.[45,46] Consequently, the observed spectra with the 532 nm laser line are similar to those with the 488 nm laser line (see Supporting Information).

The amount of blinking observed in each sample was quantified via the coefficient of variation of the integrated SERS spectra over each time series (see Methods) and is summarized in Table 1. As can be seen, while the coefficient is 22.0 ± 4.0%

Table 1. Coefficient of Variation of the SERS Spectra for the Various Samples

sample	coefficient of variation (%)
AuNRs	22.0 ± 4.0
GO/AuNRs	4.0 ± 0.5
AuNRs/RH640	30.0 ± 9.0
GO/AuNRs/RH640	7.0 ± 1.0

in the AuNR sample, it is reduced to 4.0 ± 0.5% in the GO/AuNR sample, which represents a temporal stability improvement by a 5.5 factor in the latter. Therefore, GO is found to significantly suppress blinking, facilitating molecular detection (as shown further below for RH640).

Blinking is usually a consequence of large sensitivity enhancement factors (EF) in conjunction with molecular dynamics at the nanoparticle surface, which in turn can be related to aspects such as local temperature gradients and intermolecular interactions. The theoretical EF, obtained from the electromagnetic simulations (see Methods), for the isolated and aggregated (dimer) AuNRs varies between 10^6 and 10^8 times, being sufficient to promote the observation of CTAB molecules in the hot spot. Consequently, we conclude that the blinking is caused by the CTAB dynamics, and blinking suppression in GO/AuNR samples is connected to the removal of CTA$^+$ from the hot spots. In our case, the overall heating induced by the laser can be discarded, since no significant changes in the coefficient of variation were observed within 2 orders of magnitude variation in the laser power (see the Supporting Information). Nevertheless, local heating related to the surface plasmon excitation/plasmonic absorption can still induce CTAB dynamics, being the evaluation of this phenomena, however, not a trivial task.[28,47]

Graphene Oxide/Gold Nanorod Nanocomposite as a SERS Substrate. Since GO inhibits the blinking of the CTAB molecules on AuNRs, the nanocomposite is proposed as a SERS substrate with improved stability. In a proof-of-principle experiment Rhodamine 640 was used as a probe molecule. Figure 4 compares an experimental SERS spectrum of the GO/AuNR/RH640 sample (10^{-6} M RH640 concentration) with a theoretical resonant Raman spectrum, with an excitation wavelength of 633 nm, calculated by density functional theory (DFT; see Supporting Information). There is a good match between several bands in the two spectra, confirming successful molecular probing. Differences between the spectra can be attributed to the various orientations of the RH640 molecule relative to the gold surface, as calculations were performed for the free RH640 molecule, neglecting the interaction with gold, for computational simplicity. Note that neither GO nor CTAB

DOI: 10.1021/acsphotonics.6b00109
ACS Photonics 2016, 3, 1027−1035

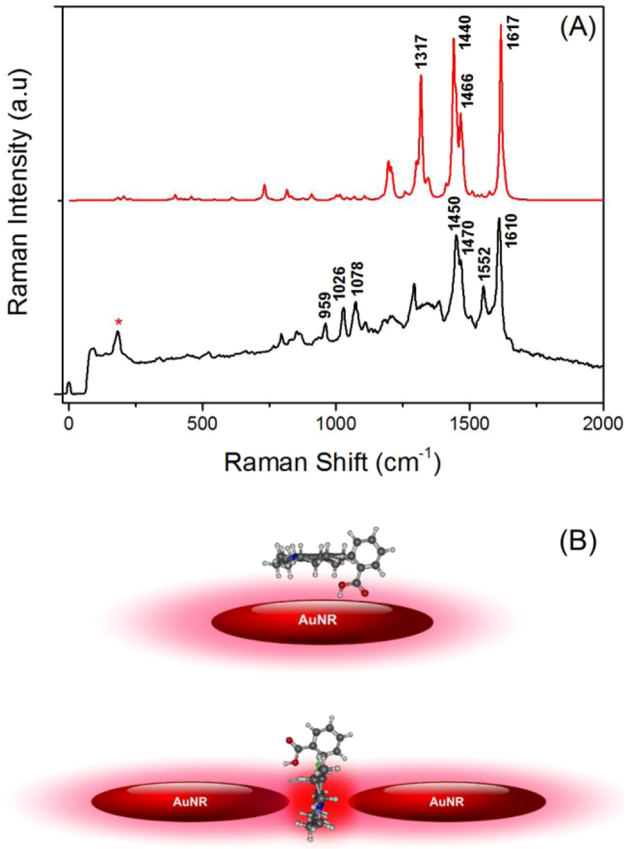

Figure 4. (a) Comparison between the RH640 resonant Raman spectra obtained via DFT numerical simulation (red) and with the SERS spectra of GO/AuNR/Rh640 sample (black). The red asterisk denotes the Au−Br stretching mode. (b) Schematic representation of the possible RH640 adsorption geometries on the gold surface.

bands interfere significantly with detection, as the GO bands are significantly broader and the Au−Br mode (the only observed CTAB mode) is removed from the spectral region of interest.

At 633 nm there is a preresonance condition with the $\pi \rightarrow \pi^*$ transition in RH640, involving the xanthene and benzene π orbitals. The excitation of this transition leads to an enhancement of 10^2, as estimated from DFT, in the normal modes, with additional contribution of the ring vibration, yielding the high intensities of the modes at 1617, 1466, 1440, and 1317 cm^{-1} in the theoretical spectra of Figure 4 (see also Table S2 in the Supporting Information). As a matter fact, when the theoretical Raman spectrum is calculated with an excitation wavelength of 1064 nm (see Supporting Information), these modes are not enhanced, confirming the contribution of the electronic resonance. Experimentally, the vibrational modes observed at 1610, 1470, and 1450 cm^{-1} are, therefore, believed to be intensified by the resonant Raman effect.

Additionally, modes at 1552, 1470, 1072, 1026, and 959 cm^{-1} present an induced transition dipole moment that is normal to the xanthene ring (see Supporting Information) and, consequently, can be enhanced via EM-SERS.[48,49] There are two possible RH640 orientations on the gold surface allowing for the enhancement of these modes: one with the xanthene ring plane parallel to the rod's axis (Figure 4b, top) and the other with the molecule between rods in an end-to-end dimer, with the ring plane perpendicular to the rods' axes (Figure 4b, bottom). In the former, the molecular dipole moment is coupled with the transverse plasmon mode, while in the latter it is coupled with the longitudinal plasmon mode. In contrast, the mode at 1317 cm^{-1} has its induced dipole within the xanthene ring plane, thus not being enhanced by the EM-SERS, while it is still visible due to the resonant Raman effect, with a slight red shift, which can be caused by its superposition with GO's D band.

A weak chemical interaction between RH640 and the gold atoms is expected due to the hard base nature of the carboxyl and furyl groups[44] and the steric hindrance of the N atoms in the xanthene ring. Also, the experimental observation of the Au−Br stretching mode at 179 cm^{-1} confirms Br^- presence on the gold nanorods surface even after the addition of RH640. Therefore, charge transfer electronic transition between the AuNRs and the dye is hardly expected, meaning that CM-SERS is negligible between RH640 and the gold atoms. Thus, the resonant Raman effect and EM-SERS are the main enhancement mechanisms associated with the strong experimental signal, which together lead to an overall estimated EF of 10^8–10^{10} (10^6–10^8 from EM-SERS times 10^2 from resonant Raman).

With such a high EF, detection at single-molecule levels is expected.[50] For confirmation of the nanocomposite's high sensitivity, experiments on lower RH640 concentrations were carried out. The spectra obtained with concentrations of 10^{-6}, 10^{-8}, and 10^{-10} M, all normalized by the highest significant peak, are shown in Figure 5. RH640 bands are clearly visible

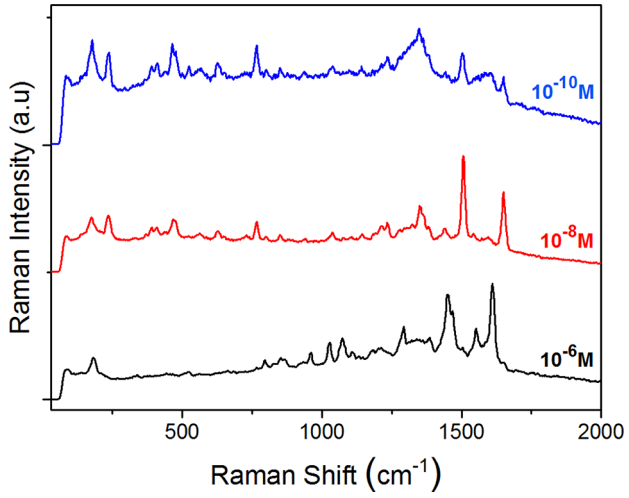

Figure 5. Spectral comparison for different RH640 concentrations on the GO/AuNR composite. All spectra have been acquired on a 0.15 mW laser power.

even for concentrations 4 orders of magnitude lower than that used for obtaining Figure 4 and well into the level at which single-molecule adhesion to gold nanoparticles is statistically expected.[51] Slight spectral shifts and differences can be observed for the lower RH640 concentrations, which can be explained from specific molecular interactions resulting from the different adsorption geometries. Indeed, Vosgrone et al. observes different spectral features for distinct Rhodamine concentrations on silver colloids.[52] While interaction with the environment plays a main role in the intensity and frequency position for low dye concentrations, inhomogeneous spectral

DOI: 10.1021/acsphotonics.6b00109
ACS Photonics 2016, 3, 1027−1035

characteristics are verified in the molecule ensemble at higher concentrations.[52]

The high estimated EFs also potentially further amplify blinking. Indeed, as can be seen in Figure 6a and in Table 1,

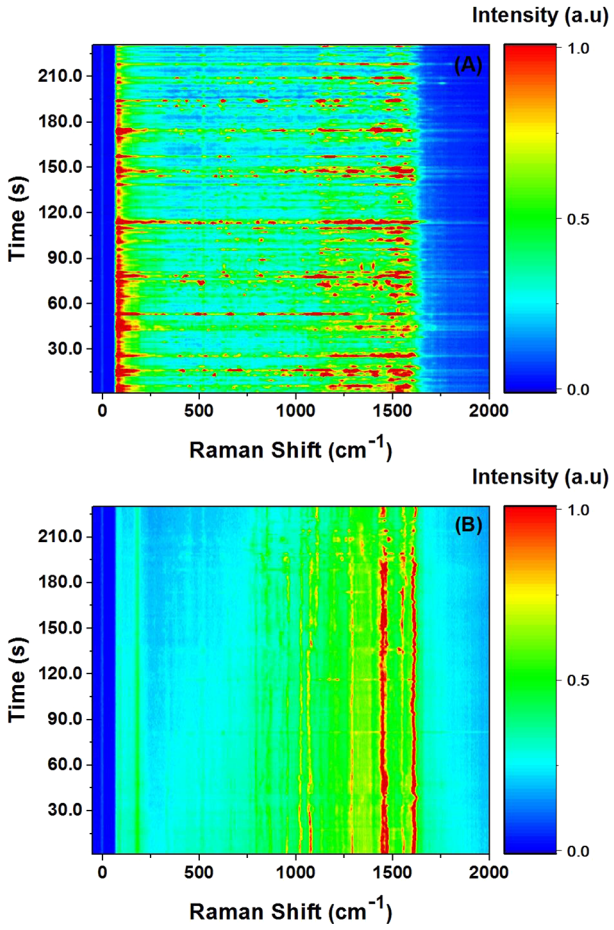

Figure 6. SERS spectra time series for (a) the AuNR/RH640 sample (laser power of 0.14 mW) and (b) the GO/AuNR/RH640 sample (laser power of 0.16 mW).

when RH640 (10^{-6} M) is added to an AuNR sample, blinking continues and seems to slightly increase (even though the increase in the coefficient of variation is within the error bars) relative to the AuNR-only case. Such an increase is possibly connected to the dynamics of adsorption/desorption of both CTA^+ and RH640 molecules within plasmonic hot spots, as Raman peaks of both molecules could be identified along a time series.

In contrast, a significantly more stable spectrum is achieved with RH640 (10^{-6} M) on the GO/AuNR substrate, as shown in Figure 6b and Table 1. In particular, Table 1 shows that the coefficient of variation in this case is over 4× lower than with the AuNR/RH640 sample and only ∼2× higher than in the SERS substrate (GO/AuNR) alone. Temporal stability measurements were also performed for the 10^{-8} M and 10^{-10} M RH640 concentrations, with blinking free operation also observed (see Supporting Information). Simultaneous high-sensitivity and high-stability operation is unusual in SERS and is a major asset of the demonstrated nanocomposite substrate. We speculate that AuNRs in the nanocomposite, which are negatively charged due to the adsorption of the Br^- ions,[10,18] attract and attach to the positively charged RH640 molecules, promoting the stable and intense SERS signal. Indeed, Hu et al. verified that anionic dyes would undergo no enhancement with GO/AuNR as a SERS substrate, further supporting the hypothesis.[18]

CONCLUSION

We presented a detailed study of the use of GO/AuNR nanocomposites for highly sensitive and stable SERS. We showed that the electrostatic attraction between GO and CTAB head groups, as well as the van der Waals interaction between the apolar CTAB tails and the GO sheets, removes CTA^+ from the AuNRs' plasmonic hotspots. As a consequence, SERS blinking, which is found to be rather strong in AuNR samples due to CTA^+ dynamics, is suppressed in GO/AuNR samples, leading to a 5-fold temporal stability improvement in the latter. As a consequence, the GO/AuNR nanocomposite compares favorably with AuNRs alone as a SERS substrate, offering plasmonic electromagnetic enhancement while suppressing blinking interference. As a proof of principle SERS experiment, Rhodamine 640 was successfully detected down to 10^{-10} M concentrations, with minimal temporal instabilities, on the GO/AuNR substrate. Our results, therefore, contribute toward a more widespread use of SERS, by demonstrating a blinking free, stable and reproducible SERS substrate.

METHODS

Gold nanorods were synthesized using a seed-mediated method.[30] The synthesis reduces $HAuCl_4$ in an aqueous solvent with $NaBH_4$ forming small nanospheres that act as nucleation seeds when added to a growth solution containing gold ions and CTAB. High quality chemicals were purchased and were prepared as follow. CTAB: dissolve 11.27 g of CTAB in 100 mL of DI water and place it into a 500 mL flask. $AgNO_3$: dissolve 13.58 mg of $AgNO_3$ in 20 mL of DI water (18.2 MΩ) and place it into a 20 mL vial. Ascorbic acid: dissolve 138.7 mg of ascorbic acid in 10 mL of DI water and place it into another 20 mL vial. $HAuCl_4$: dissolve 54.54 mg of $HAuCl_4$ in 152.5 mL of DI water and place it into a 150 mL flask. $NaBH_4$: dissolve 7.56 mg of $NaBH_4$ in 20 mL of DI water and place it into another 20 mL vial. Place the sample in the freezer after preparation; it needs to be cold before use (5 min). Bring the total volume of the CTAB solution to 155 mL using DI water.

Mix 2.5 mL of DI water and 2.5 mL $HAuCl_4$ solution into a 20 mL vial (seed solution). Stir for 5 min. Add 5 mL of the CTAB solution into the seed. Stir for 5 min (color change: yellow to orange). Add 600 μL of cold $NaBH_4$ into the seed (while stirring). Note time, τ = 0 min (color change: orange to brown). Add 7.5 mL of $AgNO_3$ to the CTAB solution. Mix with a stir bar (2 min). At τ = 2 min, stop the stir plate. Pour all the $HAuCl_4$ solution into the CTAB solution (color: orange-brownish). Mix with a stir bar (2 min). At τ = 4 min, add 2.1 mL of ascorbic acid into CTAB (solution becomes colorless). Mix with a stirring bar (1 min). At t = 5 min, add 360 μL of the seed into the CTAB solution. Shake for 30 s. Put the solution on a hot plate for 1 h at ∼45 °C. Mix with a stirring bar (∼10 rpm). After 1 h reduce heat to 25−30 °C for 2 h, then stop mixing and turn off stir bar.

After 24 h, the AuNRs are placed into a glass vial and heated to 65 °C for 10 min, the AuNR suspension is placed into six 50 mL Falcon tubes to remove the excess of CTAB from the suspension and centrifuged for 80 min at 4000g. After the first cycle, the Falcon tubes are decanted to a volume of less than 0.5

DOI: 10.1021/acsphotonics.6b00109
ACS Photonics 2016, 3, 1027−1035

mL per tube. A total of 10 mL of DI water is added to one Falcon tube, mixed thoroughly, then poured into another tube, repeating until all the AuNRs are concentrated into one tube. The AuNRs are then transferred back to one Falcon tube, diluted to 50 mL of DI water, and centrifuged for 80 min at 4000*g*. The rinsing process is repeated for a third time, with the final dilution bringing the volume to 20 mL.[53]

Graphene oxide synthesis was carried out by a modified Hummers method in a round-bottom glass flask in an iced bath. A total of 1 g of pristine graphite flakes (SP1, Bay Carbon) was added to 60 mL of sulfuric acid (Sigma-Aldrich), followed by the slow addition of 3.5 g of potassium permanganate. This system was kept under stirring for 2 h at room temperature. Subsequently, the flask was placed into the ice bath again and then 200 mL of deionized water was slowly added, followed by 2 mL of hydrogen peroxide (30 vol % on water, Sigma-Aldrich). The solid material was filtered and washed with different amounts of water, hydrochloric acid solution (10 vol %), ethanol, acetone, and DI water again. The black and solid material (graphite oxide, Gr-O) was dried under vacuum overnight. An aqueous suspension of graphite oxide was then sonicated in DI water for 1 h. The resulting brown and stable suspension was found to be graphene oxide.

Samples for SEM and Raman spectroscopy analysis were prepared on Si substrates with a 300 nm thick SiO_2 top layer, which were previously cleaned for 1 h in piranha solution (3:1, H_2SO_4/H_2O_2) and subsequently rinsed with deionized water. AuNR samples were prepared by dipping the substrate in the AuNR suspension for approximately 12 h and then drying it under gentle N_2 gas flow. For the GO/AuNR nanocomposite preparation, the substrate was first dipped in the GO suspension for 12 h and dried under N_2 flow, and then immersed in the AuNR suspension for another 12 h, finally being dried in the same manner. Similar results (not shown) were obtained with nanocomposites obtained by stirring a GO and AuNR water suspension for 72 h and then drop casting it onto the substrate. The samples containing RH640 as the probe molecule (AuNR/RH640 and GO/AuNR/RH640) were prepared by first following the preparation routes described above and then depositing a 20 μL droplet of a RH640 solution (10^{-6} M to 10^{-10} M) in deionized water, which was subsequently vacuum evaporated.

Scanning electron microscopy measurements were carried out using a JEOL 7200 field emission electron microscope. SERS measurements were conducted using a confocal Raman spectrometer (WITec Alpha 300R) with a 50× objective lens and a He−Ne 633 nm laser line, unless otherwise stated. For temporal stability analysis, 200 sequential Raman spectra were taken every 1.16 ± 0.02 s, with a 0.5 s integration time for each spectrum, resulting in an average 231 s duration time series. For quantifying Raman intensity variations within each time series, every Raman spectrum was integrated and the coefficient of variation (standard deviation(σ)/mean(μ) ratio) was calculated.

The AuNR and GO/AuNR samples were also optically characterized using a CytoViva ultraresolution imaging system.[54] It consists of a dark-field hyperspectral arrangement mounted in an Olympus BX51 microscope that spatially resolves the Rayleigh scattering spectra of individual particles. For these measurements, the AuNR sample was prepared by drop casting 2 μL of the AuNR suspension after diluting it by half with deionized water, on a NEXTERION ultraclean glass B slide (Schott). The GO/AuNR sample was prepared by dipping the ultraclean glass on the GO suspension for 3 h, drying it under N_2 flux, and then drop casting 2 μL of the AuNRs suspension on the GO film. An ultraclean NEXTERION glass coverslip (Schott) was positioned over the drop and sealed with adhesive tape; colorless fingernail polish was applied to avoid oil penetration in the sample. The dark-field optical images and the Rayleigh scattering spectra were recorded before the AuNR suspension droplet dried out in order to verify the Brownian motion of the nanorods and the influence of GO in the phenomenon.

To study the optical response of the AuNRs, numerical computations were performed using three-dimensional finite element simulations (COMSOL Multiphysics 5.1). The AuNRs (length = 60 nm, diameter = 35 nm) surrounded by vacuum were modeled as spherocylinders, placed atop a SiO_2 substrate and separated from each other and from the substrate by the approximate length of CTAB, 2.2 nm. Port geometry periodic boundary conditions were placed on the entire structure. The refractive index of gold, from 400 to 900 nm, was interpolated from literature values.[55] The AuNRs were probed with light parallel and perpendicular to the long axis of the NRs. The S_{21} element from the scattering matrix was retrieved from the simulations and used to calculate the absorbance, $\alpha x = -\log(|S_{21}|^2)$. The surface-averaged electromagnetic enhancement factor was calculated by averaging $(E/E_0)^4$ over the surface of the nanorods in the unit cell, where E is the local electric field and E_0 is the incident electric field.

RH640 molecular modeling calculations were performed using the Gaussian 09W software. The ground state geometries and the vibrational spectra were obtained by employing DFT with B3LYP hybrid functional (Becke's gradient-corrected exchange correlation in conjunction with the Lee−Yang−Parr correlation functional with three parameters).[56,57] The basis set was 6-311G(d) (scale factor of 0.962 according to the literature) and the resonant Raman spectrum was calculated using the CPHF keyword considering the excitation of 633 nm. The assignment of the vibrational spectrum was carried out by using the Gaussview 05 and Gabedit 2.4.0 softwares. The optimized geometry and nonresonant Raman spectra for the RH640 molecule can be found in the Supporting Information.

■ ASSOCIATED CONTENT

Supporting Information

The Supporting Information is available free of charge on the ACS Publications website at DOI: 10.1021/acsphotonics.6b00109.

AuNR Rayleigh spectra for the end-to-end dimer configuration; statistical spectral analysis of the dark field images; raw (not normalized) dark-field spectra for AuNR, GO/AuNR and GO samples; assignment of the CTAB and RH640 Raman bands; GO/AuNR nanocomposite spectra under different laser line excitations; coefficient of variation as a function of the incident laser power for the AuNR and GO/AuNR samples; theoretical spectrum for the RH640 molecule calculated via DFT under and out of resonance; and time series SERS measurements for different concentrations of RH640 on the nanocomposite (PDF).

■ AUTHOR INFORMATION

Corresponding Author

*E-mail: cjsdematos@mackenzie.br.

DOI: 10.1021/acsphotonics.6b00109
ACS Photonics 2016, 3, 1027−1035

Notes

The authors declare no competing financial interest.

■ ACKNOWLEDGMENTS

This work is funded by FAPESP (SPEC Project 2012/50259-8 and Thematic Project 2015/11779-4), CNPq, and MackPesquisa. P.G.V. and D.G. were supported by CNPq (Grant No. 130068/2015-2) and FAPESP (Grant No. 2015/10405-3) scholarships, respectively. I.C.S.C., G.K.B.C., and J.F. acknowledge support by the Office of Naval Research Global under ONRG-NICOP-N62909-15-1-N016. We gratefully appreciate Prof. Henrique E. Toma collaboration on providing the CytoViva Hyperspectral Dark-Field Microscope.

■ REFERENCES

(1) Stranahan, S. M.; Willets, K. A. Super-Resolution Optical Imaging of Single-Molecule SERS Hot Spots. *Nano Lett.* **2010**, *10*, 3777−3784.
(2) Bizzarri, A. R.; Cannistraro, S. Statistical Analysis of Intensity Fluctuations in Single Molecule SERS Spectra. *Phys. Chem. Chem. Phys.* **2007**, *9*, 5315−5319.
(3) Emory, S. R.; Jensen, R. A.; Wenda, T.; Han, M.; Nie, S. Re-Examining the Origins of Spectral Blinking in Single-Molecule and Single-Nanoparticle SERS. *Faraday Discuss.* **2006**, *132*, 249−259.
(4) Haran, G. Single-Molecule Raman Spectroscopy: A Probe of Surface Dynamics and Plasmonic Fields. *Acc. Chem. Res.* **2010**, *43*, 1135−1143.
(5) Le Ru, E. C.; Meyer, M.; Etchegoin, P. G. Proof of Single-Molecule Sensitivity in Surface Enhanced Raman Scattering (SERS) by Means of a Two-Analyte Technique. *J. Phys. Chem. B* **2006**, *110*, 1944−1948.
(6) Weiss, A.; Haran, G. Time-Dependent Single-Molecule Raman Scattering as a Probe of Surface Dynamics. *J. Phys. Chem. B* **2001**, *105*, 12348−12354.
(7) Wustholz, K. L.; Henry, A.-I.; Bingham, J. M.; Kleinman, S. L.; Natan, M. J.; Freeman, R. G.; Van Duyne, R. P. Exploring Single-Molecule SERS and Single-Nanoparticle Plasmon Microscopy. *Proc. SPIE* **2009**, *7394*, 739403.
(8) Le Ru, E. C.; Etchegoin, P. G. Single-Molecule Surface-Enhanced Raman Spectroscopy. *Annu. Rev. Phys. Chem.* **2012**, *63*, 65−87.
(9) Casas, J.; Venkataramasubramani, M.; Wang, Y.; Tang, L. Replacement of Cetyltrimethylammoniumbromide Bilayer on Gold Nanorod by Alkanethiol Crosslinker for Enhanced Plasmon Resonance Sensitivity. *Biosens. Bioelectron.* **2013**, *49*, 525−530.
(10) Chen, H.; Shao, L.; Li, Q.; Wang, J. Gold Nanorods and Their Plasmonic Properties. *Chem. Soc. Rev.* **2013**, *42*, 2679−2724.
(11) Wang, Y.; Aili, D.; Selegård, R.; Tay, Y.; Baltzer, L.; Zhang, H.; Liedberg, B. Specific Functionalization of CTAB Stabilized Anisotropic Gold Nanoparticles with Polypeptides for Folding-Mediated Self-Assembly. *J. Mater. Chem.* **2012**, *22*, 20368−20373.
(12) Fabris, L. Gold-Based SERS Tags for Biomedical Imaging. *J. Opt.* **2015**, *17*, 114002.
(13) Fontana, J.; Livenere, J.; Bezares, F. J.; Caldwell, J. D.; Rendell, R. Large Surface-Enhanced Raman Scattering from Self-Assembled Gold Nanosphere Monolayers. *Appl. Phys. Lett.* **2013**, *102*, 201606.
(14) Stiles, P. L.; Dieringer, J. A.; Shah, N. C.; Duyne, R. P. Van. Surface-Enhanced Raman Spectroscopy. *Annu. Rev. Anal. Chem.* **2008**, *1*, 601−625.
(15) Ling, X.; Xie, L.; Fang, Y.; Xu, H.; Zhang, H.; Kong, J.; Dresselhaus, M. S.; Zhang, J.; Liu, Z. Can Graphene Be Used as a Substrate for Raman Enhancement? *Nano Lett.* **2010**, *10*, 553−561.
(16) Yu, X.; Cai, H.; Zhang, W.; Li, X.; Pan, N.; Luo, Y.; Wang, X.; Hou, J. G. Tuning Chemical Enhancement of SERS by Controlling the Chemical Reduction of Graphene Oxide Nanosheets. *ACS Nano* **2011**, *5*, 952−958.
(17) Yin, P. T.; Shah, S.; Chhowalla, M.; Lee, K.-B. Design, Synthesis, and Characterization of Graphene−Nanoparticle Hybrid Materials for Bioapplications. *Chem. Rev.* **2015**, *115*, 2483−2531.
(18) Hu, C.; Rong, J.; Cui, J.; Yang, Y.; Yang, L.; Wang, Y.; Liu, Y. Fabrication of a Graphene Oxide-Gold Nanorod Hybrid Material by Electrostatic Self-Assembly for Surface-Enhanced Raman Scattering. *Carbon* **2013**, *51*, 255−264.
(19) Pan, H.; Low, S.; Weerasuriya, N.; Shon, Y.-S. Graphene Oxide-Promoted Reshaping and Coarsening of Gold Nanorods and Nanoparticles. *ACS Appl. Mater. Interfaces* **2015**, *7*, 3406−3413.
(20) Wang, P.; He, H.; Jin, Y. Shape Transformation and Visible Region Plasmonic Modulation of Silver Nanoplates by Graphene Oxide. *Small* **2012**, *8*, 3438−3442.
(21) Hou, H.; Wang, P.; Zhang, J.; Li, C.; Jin, Y. Graphene Oxide-Supported Ag Nanoplates as LSPR Tunable and Reproducible Substrates for SERS Applications with Optimized Sensitivity. *ACS Appl. Mater. Interfaces* **2015**, *7*, 18038−18045.
(22) Thickett, S. C.; Zetterlund, P. B. Preparation of Composite Materials by Using Graphene Oxide as a Surfactant in Ab Initio Emulsion Polymerization Systems. *ACS Macro Lett.* **2013**, *2*, 630−634.
(23) Cote, L. J.; Kim, J.; Zhang, Z.; Sun, C.; Huang, J. Tunable Assembly of Graphene Oxide Surfactant Sheets: Wrinkles, Overlaps and Impacts on Thin Film Properties. *Soft Matter* **2010**, *6*, 6096.
(24) Wang, Z.; Rothberg, L. J. Origins of Blinking in Single-Molecule Raman Spectroscopy. *J. Phys. Chem. B* **2005**, *109*, 3387−3391.
(25) Andersen, P. C.; Jacobson, M. L.; Rowlen, K. L. Flashy Silver Nanoparticles. *J. Phys. Chem. B* **2004**, *108*, 2148−2153.
(26) Dembereldorj, U.; Choi, S. Y.; Ganbold, E.-O.; Song, N. W.; Kim, D.; Choo, J.; Lee, S. Y.; Kim, S.; Joo, S.-W. Gold Nanorod-Assembled PEGylated Graphene-Oxide Nanocomposites for Photothermal Cancer Therapy. *Photochem. Photobiol.* **2014**, *90*, 659−666.
(27) Jacobson, M. L.; Rowlen, K. L. Photo-Dynamics on Thin Silver Films. *Chem. Phys. Lett.* **2005**, *401*, 52−57.
(28) Mezni, A.; Dammak, T.; Fkiri, A.; Mlayah, A.; Abid, Y.; Smiri, L. S. Photochemistry at the Surface of Gold Nanoprisms from Surface-Enhanced Raman Scattering Blinking. *J. Phys. Chem. C* **2014**, *118*, 17956−17967.
(29) Doering, W. E.; Nie, S. Single-Molecule and Single-Nanoparticle SERS: Examining the Roles of Surface Active Sites and Chemical Enhancement. *J. Phys. Chem. B* **2002**, *106*, 311−317.
(30) Nikoobakht, B.; El-sayed, M. A. Preparation and Growth Mechanism of Gold Nanorods (NRs) Using Seed-Mediated Growth Method. *Chem. Mater.* **2003**, *15*, 1957−1962.
(31) Domingues, S. H.; Kholmanov, I. N.; Kim, T.; Kim, J.; Tan, C.; Chou, H.; Alieva, Z. A.; Piner, R.; Zarbin, A. J. G.; Ruoff, R. S. Reduction of Graphene Oxide Films on Al Foil for Hybrid Transparent Conductive Film Applications. *Carbon* **2013**, *63*, 454−459.
(32) Caires, A.; Alves, D. C. B.; Ferlauto, A.; Fantini, C.; Ladeira, L. O. One-Pot in Situ Photochemical Synthesis of Graphene Oxide/gold Nanorods Nanocomposite for Surface-Enhanced Raman Spectroscopy. *RSC Adv.* **2015**, *5*, 46552−46557.
(33) Lee, Y. H.; Polavarapu, L.; Gao, N.; Yuan, P.; Xu, Q. Enhanced Optical Properties of Graphene Oxide - Au Nanocrystal Composites. *Langmuir* **2012**, *28*, 321−326.
(34) Zedan, A. F.; Moussa, S.; Terner, J.; Atkinson, G.; El-shall, M. S. Ultrasmall Gold Nanoparticles Anchored to Graphene and Enhanced Photothermal Effects by Laser Irradiation of Gold Nanostructures in Graphene Oxide Solutions. *ACS Nano* **2013**, *7*, 627−636.
(35) Das, K.; Maiti, S.; Ghosh, M.; Mandal, D.; Das, P. K. Graphene Oxide in Cetyltrimethylammonium Bromide (CTAB) Reverse Micelle: A Befitting Soft Nanocomposite for Improving Efficiency of Surface-Active Enzymes. *J. Colloid Interface Sci.* **2013**, *395*, 111−118.
(36) Funston, A. M.; Novo, C.; Davis, T. J.; Mulvaney, P. Plasmon Coupling of Gold Nanorods at Short Distances and in Different Geometries. *Nano Lett.* **2009**, *9*, 1651−1658.
(37) Burda, C.; Chen, X.; Narayanan, R.; El-Sayed, M. A. Chemistry and Properties of Nanocrystals of Different Shapes. *Chem. Rev.* **2005**, *105* (4), 1025−1102.
(38) Link, S.; El-Sayed, M. A. Spectral Properties and Relaxation Dynamics of Surface Plasmon Electronic Oscillations in Gold and

DOI: 10.1021/acsphotonics.6b00109
ACS Photonics 2016, 3, 1027−1035

Silver Nanodots and Nanorods. *J. Phys. Chem. B* **1999**, *103* (40), 8410−8426.
(39) Link, S.; El-Sayed, M. a. Optical Properties and Ultrafast Dynamics of Metallic Nanocrystals. *Annu. Rev. Phys. Chem.* **2003**, *54*, 331−366.
(40) Boca, S. C.; Astilean, S. Detoxification of Gold Nanorods by Conjugation with Thiolated Poly(ethylene Glycol) and Their Assessment as SERS-Active Carriers of Raman Tags. *Nanotechnology* **2010**, *21*, 235601.
(41) Eftekhari, F.; Lee, A.; Kumacheva, E.; Helmy, a S. Examining Metal Nanoparticle Surface Chemistry Using Hollow-Core, Photonic-Crystal, Fiber-Assisted SERS. *Opt. Lett.* **2012**, *37*, 680−682.
(42) Moore, A. A.; Jacobson, M. L.; Belabas, N.; Rowlen, K. L.; Jonas, D. M. 2D Correlation Analysis of the Continuum in Single Molecule Surface Enhanced Raman Spectroscopy. *J. Am. Chem. Soc.* **2005**, *127*, 7292−7293.
(43) Meng, W.; Gall, E.; Ke, F.; Zeng, Z.; Kopchick, B.; Timsina, R.; Qiu, X. Structure and Interaction of Graphene Oxide − Cetyltrimethylammonium Bromide Complexation. *J. Phys. Chem. C* **2015**, *119*, 21135−21140.
(44) Pearson, R. G. Absolute Electronegativity and Hardness Correlated with Molecular Orbital Theory. *Proc. Natl. Acad. Sci. U. S. A.* **1986**, *83*, 8440−8441.
(45) Arnold, M. D.; Blaber, M. G. Optical Performance and Metallic Absorption in Nanoplasmonic Systems. *Opt. Express* **2009**, *17*, 3835−3847.
(46) Maier, S. A. *Plasmonics: Fundamentals and Applications*; Springer, 2007.
(47) Kang, T.; Hong, S.; Choi, Y.; Lee, L. P. The Effect of Thermal Gradients in SERS Spectroscopy. *Small* **2010**, *6*, 2649−2652.
(48) Gao, X.; Davies, J. P.; Weaver, M. J. Test of Surface Selection Rules for Surface-Enhanced Raman Scattering: The Orientation of Adsorbed Benzene and Monosubstituted Benzenes on Gold. *J. Phys. Chem.* **1990**, *94*, 6858−6864.
(49) Moskovits, M. Surface Selection Rules. *J. Chem. Phys.* **1982**, *77*, 4408.
(50) Etchegoin, P. G.; Le Ru, E. C. A Perspective on Single Molecule SERS: Current Status and Future Challenges. *Phys. Chem. Chem. Phys.* **2008**, *10*, 6079−6089.
(51) Liu, H.; Zhang, L.; Lang, X.; Yamaguchi, Y.; Iwasaki, H.; Inouye, Y.; Xue, Q.; Chen, M. Single Molecule Detection from a Large-Scale SERS-Active Au79Ag21 Substrate. *Sci. Rep.* **2011**, *1*, 112.
(52) Vosgrçne, T.; Meixner, A. J. Spectroscopy of Xanthene Dyes: From the Ensemble to Single Molecules. *ChemPhysChem* **2005**, *6*, 154−163.
(53) Fontana, J. P. Self-Assembly and Characterization of Anisotropic Metamaterials. *Ph.D. Thesis*, Kent State University, 2011.
(54) Vainrub, A.; Pustovyy, O.; Vodyanoy, V. Resolution of 90 Nm (λ/5) in an Optical Transmission Microscope with an Annular Condenser. *Opt. Lett.* **2006**, *31*, 2855−2857.
(55) Edward, P. D. Handbook of Optical Constants of Solids. *Acad. Press* **1998**, 3.
(56) Perdew, J. P. Density-Functional Approximation for the Correlation Energy of the Inhomogeneous Electron Gas. *Phys. Rev. B: Condens. Matter Mater. Phys.* **1986**, *33*, 8822−8824.
(57) Becke, A. D. Density-Functional Exchange-Energy Approximation with Correct Asymptotic Behavior. *Phys. Rev. A: At., Mol., Opt. Phys.* **1988**, *38*, 3098−3100.

DOI: 10.1021/acsphotonics.6b00109
ACS Photonics 2016, 3, 1027−1035